INTERPRETED FAULTING PATTERNS IN NORTHEAST ALBERTA USING HIGH RESOLUTION AEROMAGNETIC DATA

M. E. Best[1], H. J. Abercrombie[2] and J. W. Peirce[3]

Canadian Journal of Exploration Geophysicists, 1998

ABSTRACT

A high resolution aeromagnetic survey was flown north of Fort McMurray in northern Alberta where the depth to Precambrian basement is shallow. The objective of the survey was to map the faulting patterns in the crystalline basement and the sediments lying above it. The magnetic sources in the survey area, being relatively close to the magnetometer, produce strong magnetic anomalies. The shallow magnetic sources, combined with high-quality survey specifications (tight line spacing, low ground clearance and careful flight line leveling), make first and second vertical derivatives effective for mapping faults and contacts. NE-SW and NW-SE faults are observed to offset north-south lineaments associated with basement shearing and lithologic contacts. The NW-SE faults offset the NE-SW faults, providing evidence that the NW faults are the younger of the two sets. These two fault directions are common throughout northern Alberta, but to our knowledge this is the first time their relative age could be determined.

INTRODUCTION

A high resolution aeromagnetic (HRAM) survey was flown north of Fort McMurray in northern Alberta (Figure 1), where the depth to Precambrian basement is shallow (less than 600 m below the ground surface). The objective of the survey was to map magnetic features in the crystalline basement and the overlying sediments of the Western Canada Sedimentary Basin and to delineate faulting patterns within these two distinct units. The Taltson Magmatic Arc (large red coloured magnetic zone in Figure 2), a highly magnetic terrane, underlies the survey area except at the extreme eastern edge. For reference, the Syncrude plant is located just south of the survey area. Although numerous shallow wells have been drilled within the area for tar sand exploration, few of the holes have casing so cultural contamination is minimal. The data were edited and leveled and then used to generate a variety of map and profile outputs. This paper is devoted to a discussion of how these products were generated and used to determine the faulting patterns within the region.

SURVEY SPECIFICATIONS

A total of 23,013 line kilometers of data were collected by World Geoscience during the summer of 1997. The survey was flown in drape mode using differential GPS at an average ground clearance of 100 m. Traverse line spacing was 300 m in the east-west direction and 600 m for the north-south tie lines.

The acquisition aircraft was fitted with a stinger mounted, Scintrex V-201 H-8 optically pumped, cesium vapor magnetometer with a sample interval of 0.1 second (equivalent to a sample interval on the ground between 6 m and 8 m). Aircraft navigation was carried out using a GPS receiver unit coupled to a real-time differential GPS system. The resulting corrected position data were fed to both a navigation computer and a data acquisition computer. The output of the navigation computer was used for real-time navigation by the pilot in X, Y and Z to allow flying a preplanned drape surface. The data on tape was combined with the recorded GPS base station data to provide a post-processed differentially corrected flight path with an estimated accuracy of ± 5 m or better

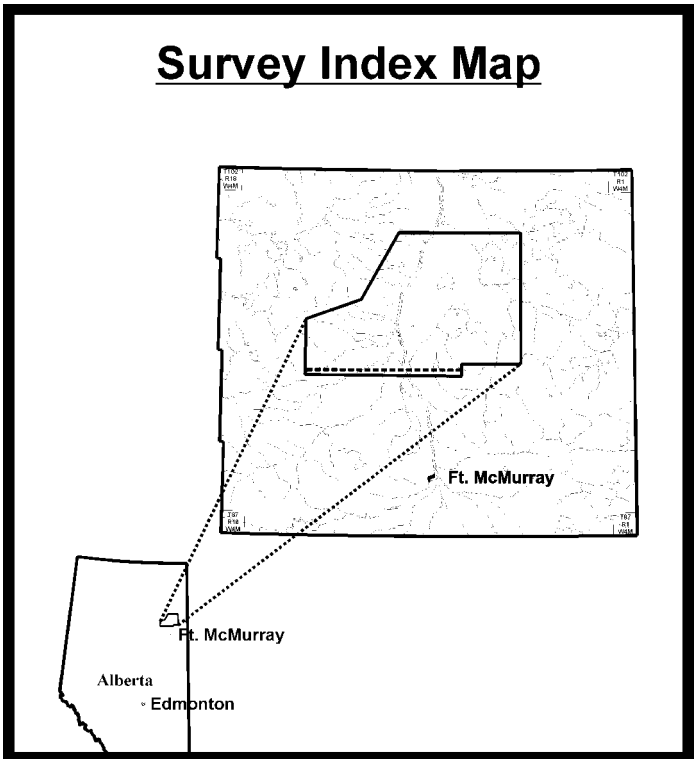

Figure 1: Map showing the location of the survey area in northern Alberta. The dashed line is the location of the MagProbe profile discussed in Figure 6.

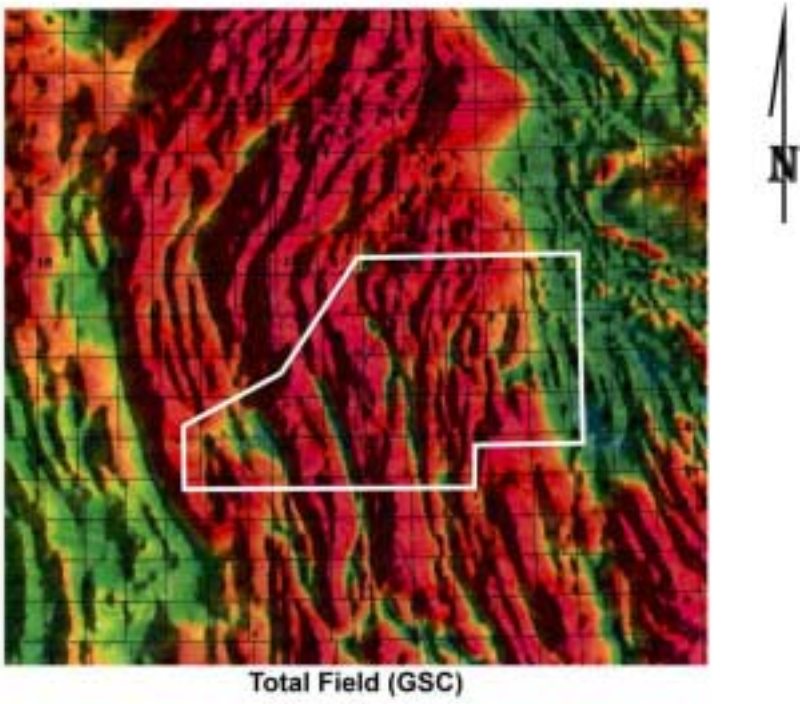

F**igure 2**: Blowup of the Geological Survey of Canada's regional aeromagnetic map of Alberta showing the area encompassing the survey area (Geophysical Data Centre, 1997).

A diurnal base station using a Scintrex H-8 magnetometer was maintained in a magnetically quiet location near the survey area to ensure that data were not acquired during magnetically noisy periods. The data were adjusted by the contractor to compensate for diurnal variations. The geomagnetic activity was observed to be low, and no magnetic storms were noted during the survey.

Data processing also included a correction for the geomagnetic gradient using the International Geomagnetic Reference Field (IGRF) at the exact time and position of each data point.

CULTURAL EDITING

Cultural editing of the leveled and corrected magnetic data from World Geoscience was carried out by Geophysical Exploration & Development Corporation (GEDCO). The magnetic data were first gridded at 100 m. A high-frequency filtered grid of the magnetic data was plotted at 1:30,000 to assist in the cultural editing process. Locations of known wells, pipelines, culture and flight lines were superimposed on the filtered magnetic data. The videotapes from the downward looking camera mounted on the aircraft were carefully reviewed, and any coincidence between man-made culture and these high-frequency magnetic anomalies was noted and plotted on the map. This approach gives a two-dimensional perspective of the cultural anomaly so that editing can be consistent on adjacent lines.

Profiles of the survey data were carefully examined using a workstation. Sections of the profile contaminated by cultural signal were removed, and a smooth function was interpolated across the resulting gap to obtain a continuous profile. Hassan, et al. (1998, this issue) discuss various approaches to cultural editing, including some examples from this data set.

In areas with significant cultural contamination releveling is required because the mis-ties at tie line/traverse line intersections are disturbed by the removal and/or smoothing of cultural anomalies. In this survey there was relatively little culture to remove. Although many shallow wells were indicated on the map, most had no casing and hence had no magnetic effect on the data. Consequently, no releveling was required.

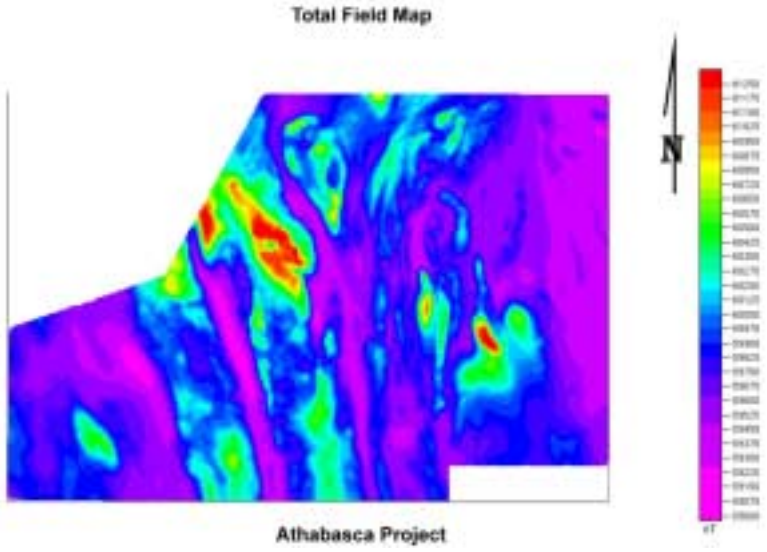

Figure 3: Total magnetic field map after reduction to the pole, leveling and cultural editing. Diurnal and IGRF corrections have been applied, as well as a filter to reduce high-frequency noise. The data were gridded at a spacing of 100 m

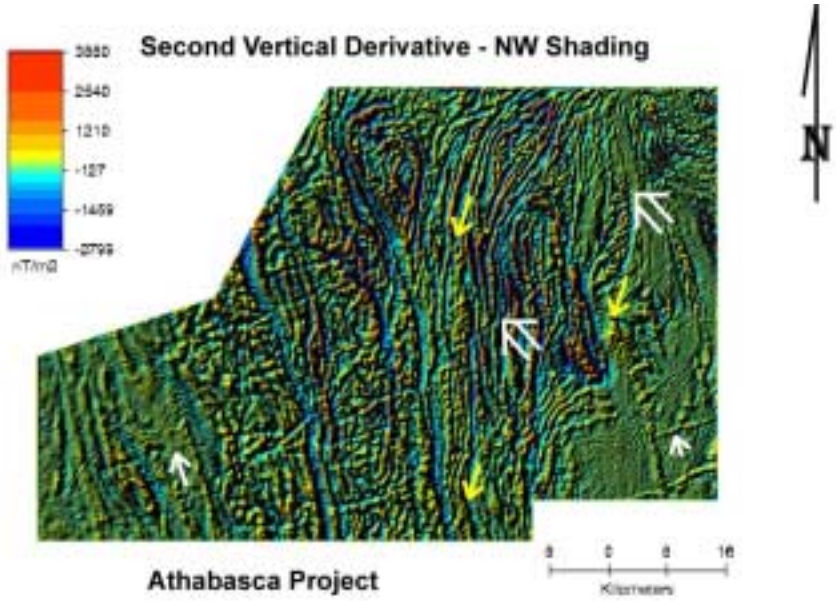

Figure 4: Second vertical derivative map of the total magnetic field (Figure 3) with sun shading from the northwest. This shading highlights NE-SW lineaments. The white arrows point to the locations of some of the WSW-ENE lineaments; the double white arrows point to the location of some of the NE-SW lineaments; and the yellow arrows point to some of the NW-SE lineaments. The NW-SE lineaments do not show up well on this image because of the northwesterly illumination. The major NE-SW lineament highlighted by the double white arrows is offset in a left lateral sense by a NW-SE fault just to the SW of the center double white arrow.

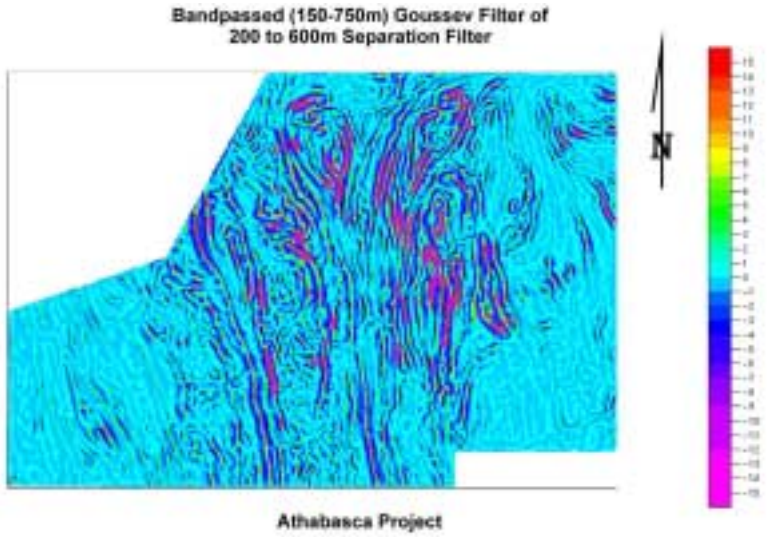

Figure 5: Cascaded Goussev filter map of the total magnetic field (Figure 3). A separation filter of 200-600 m (Jacobsen, 1987) was applied to the magnetic field before the Goussev filter. The separation filter focuses on magnetic sources in the shallow basement and sediments. The Goussev filter sharpens magnetic contacts and other lineaments and is similar to the gradient operators. A bandpass of 150-750 m was applied after the Goussev filter.

PROCESSING

The leveled and culturally edited data were filtered to remove any high-frequency noise that may contaminate the derivative maps. The data were then reduced to the pole using the following values of the earth's magnetic field in the survey area: magnitude = 59,945 nT; declination = 20.2 and inclination = 79.3. Reduction to the pole applies a phase shift to center the magnetic anomalies over their causative bodies. In northern latitudes magnetic positives are shifted slightly northward by this process. The resulting total magnetic field map is presented in Figure 3. This gridded data set was subsequently used to generate bandpass, derivative, upward continued and separation filter maps, as well as combinations of these. Sun shading was applied to several filtered maps to enhance particular lineaments. Although many different filters were applied, we shall discuss only the following in this paper:

- The second vertical derivative of the magnetic data is an effective tool for focusing on shallow (short wavelength) magnetic features. Sun positioning from the northeast and northwest was used to enhance northwest and northeast lineaments respectively. Figure 4 is an example of sun shading from the northwest.
- A cascaded Goussev filter (Goussev filter of a 200-600 m separation filter) was applied to the magnetic data to enhance edges of contacts and lineaments (Figure 5). The separation filter (Jacobsen, 1987) focuses on anomalies originating just below the top of the Precambrian basement and within the sediments just above the basement. The Goussev filter reduces noise and sharpens the location of magnetized faults/contacts and other magnetic lineaments. It is a technique based on cascading certain gradient filters (see Goussev et al., 1998, this issue, for further examples and discussion).

In addition to image processing, depth estimates using Werner and Euler deconvolution (Werner, 1953; Jain, 1976; Thompson, 1982; Ku and Sharpe, 1983; Reid et al., 1990) were made on every profile with the specific objective of mapping fault/contact lineaments.

INTERPRETATION

Strong magnetic sources in the shallow basement, combined with the high-resolution aeromagnetic survey, provide an ideal opportunity to use second vertical derivative maps effectively. Derivative maps enhance shallow (short wavelength) magnetic features as well as any noise in the data. Fortunately noise is weaker than the magnetic sources in this survey. The derivative maps can therefore be used to sharpen the edges of magnetic anomalies and to better define their location. The cascaded Goussev filter with a separation filter of 200 to 600 m is also effective at enhancing short wavelength (shallow basement and sediment) magnetic features.

Many northerly trending magnetic lineaments are visible on the second vertical derivative and cascaded Goussev filter maps (Figs. 4 and 5). The lineaments probably follow lithologic contacts in the basement and/or basement shearing trends. Northeast-southwest and northwest-southeast fault trends can be seen to offset the northerly trending lineaments more clearly on the second vertical derivative map than on the cascaded Goussev filter map. On the cascaded Goussev filter map these faults tend to show up as weak discontinuities in the north-south lineaments. The northeast-southwest fault going from the lower left corner of the map to the upper right corner is a major feature that can even be traced on the total magnetic field map (Figure 3). Figure 4 shows the northwest trending faults offsetting the northeast trending faults in this area, indicating the northwest-southeast faults are the younger of the two sets. These two fault directions are common throughout northern Alberta (O'Connell, 1994; Wright et al., 1994; Ross et al., 1994), but this is the only example we know of where their relative age can be determined. This information can be used to infer the relative age of the same fault trends further to the west. A few approximately east-west faults can also be seen on the second vertical derivative map.

Depths estimated from Werner deconvolution (Werner, 1953) were obtained from both the total magnetic field and the horizontal gradient of the magnetic field. Depth estimates obtained from the total field assume the magnetic body is a thin dipping dike, while depth estimates obtained from the horizontal gradient assume the magnetic body is a contact between two geological rock units of different susceptibility. Both models assume the strike direction of the magnetic body is infinite.

In theory, Werner deconvolution should provide an estimate of the depth to the top of the magnetic body (thin dike or contact). Extensive modeling (Peirce et al., in press; also see Fig. 1 of Goussev et al., this volume) of a variety of different bodies, however, has shown that depth solutions are spread out in the vertical direction for models with heterogenous magnetization. In the special case where the body is uniformly magnetized and vertical, the depth solutions cluster or are smeared out over some distance near the top of the body. The amount of spreading appears to depend on several factors: 1) the choice of deconvolution parameters; 2) the amount of noise; 3) the distribution of magnetization within the magnetic body; and 4) the shape of the magnetic body.

Our modeling has shown that the depth estimates (in both vertical and lateral directions) are directly related to the shape and distribution of magnetization. We have observed that depth solutions spread out along the depth extent of dikes and contacts, either when the magnetization is depth-dependent and/or the magnetic body is non-vertical. Apparently the depth solutions cluster around the tops of a number of short segments that make up the magnetic body. These short segments appear to represent segments of constant magnetization and/or *equivalent* vertical segments of a non-vertical body. The deconvolution parameters used in the modeling were the same as those used on field data, so a direct comparison could be made between model and real data.

Euler depth solutions (Reid at al., 1990) were obtained from the total magnetic field. The depth estimates should again provide an estimate of the depth to the top of the magnetic body. The actual depth also depends on the choice of the structural index "n" that appears in the theoretical development of the Euler method (n can have values between 0 to 3). Higher values of the structural index (2 to 3) are more representative of two- and three-dimensional magnetic bodies, while lower values (0.5 to 1.5) are more representative of contacts and faults. Regardless of the choice of structural index, our modeling has shown the depth estimates still spread out along the depth extent of magnetic dikes and contacts in a manner very similar to the Werner depth estimates.

Modeling has shown that a relationship exists between the distribution of depth solutions and the magnetic bodies that produce these distributions. We therefore believe that the distribution of depth solutions (for example the red and blue lines on Figure 6) can outline the approximate shape and extent of magnetic bodies.

Intra-sedimentary faults interpreted from the depth solution profiles generally follow the direction of mapped basement faults, although they are not necessarily coincident. Authigenic pyrrhotite forming in fractures may be a possible cause of magnetic features associated with the intra-sedimentary faults (Peirce et al., 1998).

Figure 6 is an example of a depth estimate profile for an east-west flight line. A well near the western end of this line (09-34-094-14W4), which reached Precambrian basement at a depth of 186 m below sea level, provides depth control. The well was projected approximately 6 km south onto the line. The horizontal black line at depths between 320 m and 50 m below sea level is the interpreted Precambrian surface. The discrepancy between the interpreted depth to basement (approximately 320 m below sea level) and the depth to basement from the well (186 m below sea level) is not that unusual for magnetic depth estimation since the accuracy of the interpreted depth to basement is ±50 m at best. Combine this with the fact the basement gradient is quite large in this area, thus over a distance of 6 km the basement depth can change by up to 100 m. On the other hand, the well depth to basement was used to control the interpreted basement depth for those regions of magnetic profiles that were close to the well.

We have developed the indicators below to determine the depth to the Precambrian basement using Euler and Werner depth solutions.

- A set of depth estimates that map out horizontally along a surface near the expected depth to basement.
- Frequently there is a small zone with no depth solutions just above the basement (typically 100-200 m in thickness).
- Deeper faults within the basement stop abruptly along a surface near the expected depth to basement.
- Shallower faults within the sediments stop abruptly along a surface near the expected depth to basement.
- Basement faults sometimes dip in one direction, and the associated intra-sedimentary faults dip in a different direction. These dips are determined from the trace of the depth solutions.

After the Precambrian surface is interpreted, the faults and contacts can be identified as basement or intra-sedimentary. Several horizontal magnetic bodies within the basement are delineated by the depth estimates (the horizons coloured orange are in the basement, and the horizons coloured blue are in the sediments). These regions may contain sources of mineralized fluids that can move upward along basement faults into the sediments (Peirce et al., 1998). Similar features appear within the sedimentary package, perhaps suggesting that magnetizing fluids may move horizontally outward from the intra-sedimentary faults.

Intra-sedimentary faults: 1) may be coincident with basement faults; 2) may be present where there are no basement faults; and 3) may not be present where there are basement faults. All three of these situations occur in the survey area. These different conditions furnish information about fault genesis and relative ages that may help to interpret basement and sedimentary structure and to determine fluid migration pathways.

As mentioned earlier this data set provides information on faulting patterns and relative ages because the magnetic sources are close to the magnetometer and the magnetic data is of high quality. Figure 7 illustrates what happens to the magnetic field after upward continuing the magnetic data in Figure 3 to 1000 m (1100 m above the ground). This is equivalent to having an additional 1000 m of non-magnetic sediments overlying the present surface. The data now looks smoother and more regional. Interestingly, the upward continued data appears to contain more detailed information than the GSC data in Figure 2 which was collected 300 m above the ground. We believe this is due to the much closer traverse line spacing and 3:1 traverse/control line ratio in our detailed survey as compared with several kilometer spacing of traverse lines with only a few control lines for the regional GSC survey. Figure 8 is the second vertical derivative of the upward continued magnetic field. Much of the detail evident in Figure 4 is lost when the magnetic sources are 1000 m further from the magnetometer. The northeast-southwest fault mentioned earlier is still visible but some of the more subtle east-west and northwest-southeast faults/contacts are attenuated.

This exercise demonstrates the deterioration of the magnetic structural information with increasing distance between the magnetic sources and the magnetometer. Note upward continuation by 1000 m is not the same as flying over an area where there is an additional 1000 m of sediments above the basement that contain magnetic sources. In this case the magnetic sources within the shallower sediments could produce strong magnetic anomalies.

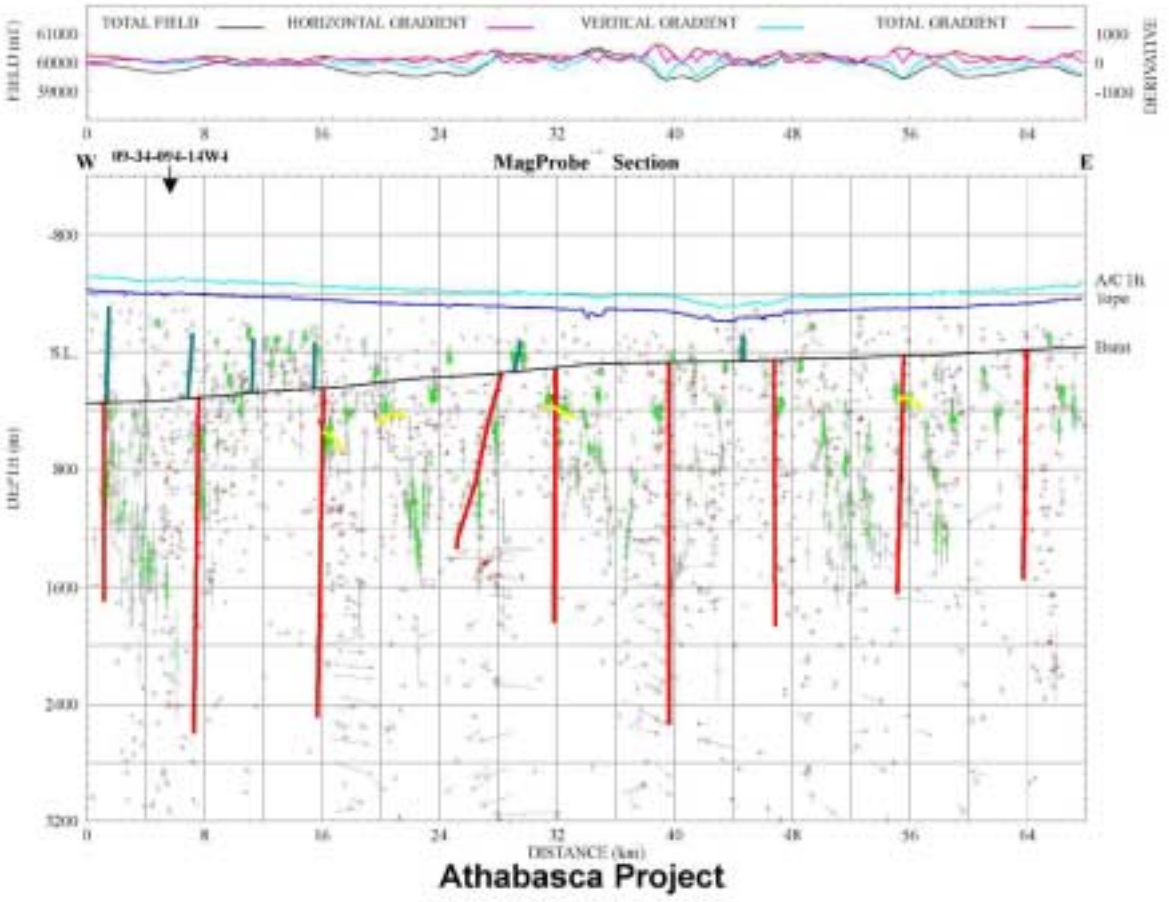

Figure 6: Example of an east-west profile showing depth estimates computed from Euler and Werner deconvolution. The upper profiles are the total magnetic field (black line) and several gradient traces (coloured lines). In the depth section, the red depth solutions are from Werner deconvolution and the green from Euler estimates. The light blue horizontal line is the measured flight profile of the aircraft, and the dark blue horizontal line is the topography along the profile. The blue vertical lines are interpreted intra-sedimentary faults, and the red vertical lines are interpreted basement faults/ contacts. The sub-horizontal black line is the interpreted Precambrian surface. The horizontal orange lines are interpreted magnetic bodies in the basement. The well (09-34-094-14W4) shown in the figure is projected from approximately 6 km north onto this profile. Precambrian basement at the well is at a depth of 186 m below sea level . The location of this line is given in Figure 1.

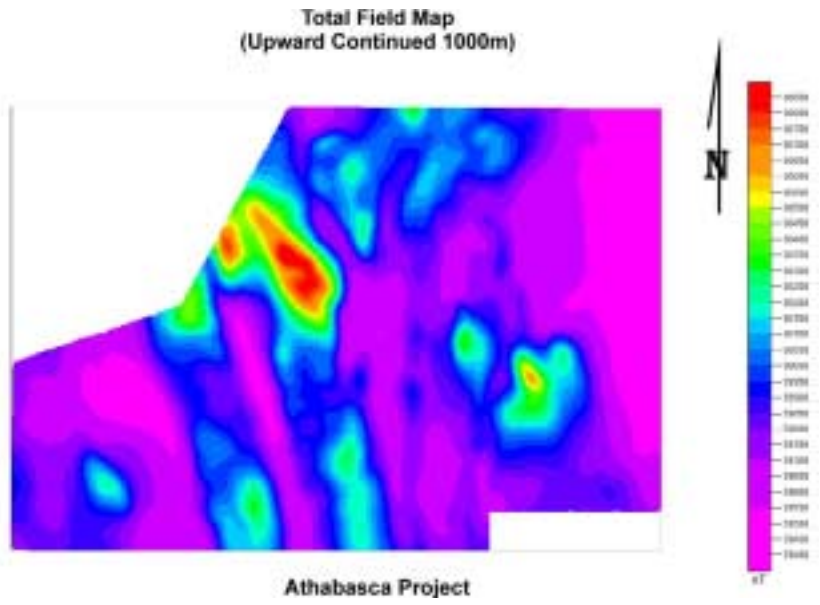

Figure 7: Upward continuation of the magnetic field (Figure 3) by 1000 m.

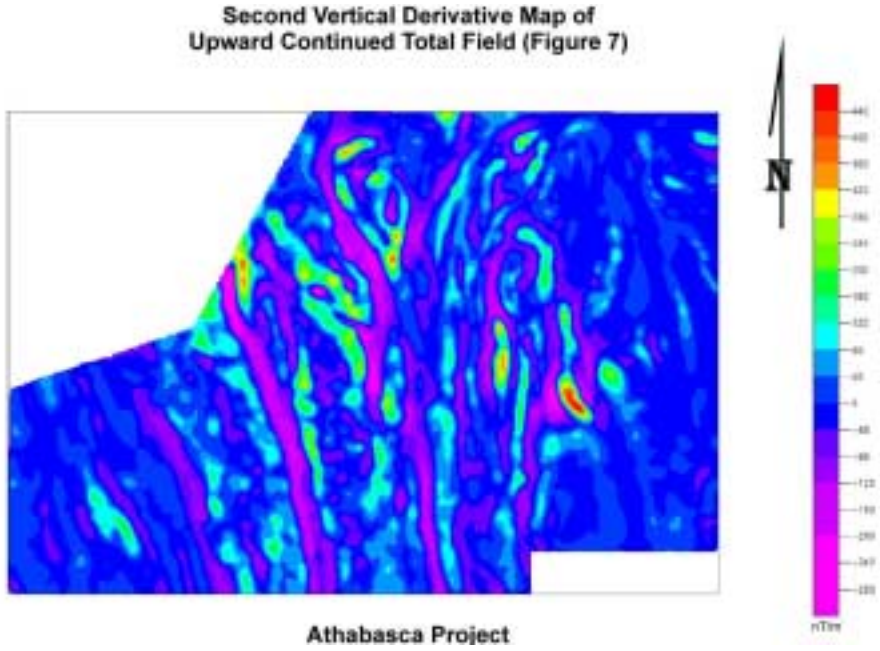

Figure 8: Second vertical derivative of the upward continued magnetic field (Figure 7).

CONCLUSIONS

The strong magnetic sources, combined with high-quality acquisition and processing, produced an aeromagnetic data set that was of exceptionally high quality for interpretation. Fault trends and relative age relationships could be determined from the vertical derivative maps because the noise was significantly reduced and magnetic lineaments were clearly observed in the data.

Upward continuing the data by 1000 m illustrates how magnetic data can change from detailed to general, depending on the average distance from magnetic sources. Comparison of the original and the upward continued second vertical derivative maps (Figures 4 and 8) illustrates this point quite well. Although much of the magnetic detail is lost, the overall structural trends still remain.

This study emphasizes the importance of flying at the minimum ground clearance possible. It also demonstrates that closer line spacing with more control lines can provide more detailed information even at a regional level.

The high-quality magnetic data provided the first published evidence, at least to our knowledge, for the relative age of the NE-SW and NW-SE fault trends in northern Alberta. Such information could provide important constraints for petroleum and mineral exploration within the area. Finally the Euler and Werner depth estimates give additional constraints on the depth to the Precambrian basement and on the location of basement and intra-sedimentary faults and magnetic bodies.

REFERENCES

Geophysical Data Centre, 1997, Regional aeromagnetic map of Alberta: Geological Survey of Canada, Natural Resources Canada.

Goussev, S. A., Charters R. A., and Hassan, H. H., 1998, HRAM fault interpretation using MagProbe depth estimates and non-traditional filtering: Can. J. Expl. Geoph., this volume.

Hassan, H. H., Peirce, J. W., Pearson, W. C., and Pearson, M. J., 1998, Cultural editing of HRAM data: comparison of existing techniques, Can. J. Expl. Geoph. , this volume.

*Jacobsen, B., 1987, A case for upward continuation as a standard separation filter for potential-field maps: Geophysics, **52**, 1138-1148.*

*Jain, S. 1976, An automatic method of direct interpretation of magnetic profiles: Geophysics, **41**, 531-541.*

*Ku, C. C., and Sharpe, S. A., 1983, Werner deconvolution for automated magnetic interpretation and its refinement using Marquardt's inverse modeling: Geophysics, **48**, 754-774.*

O'Connell, S. C., 1994, Geological history of the Peace River Arch: in Geological Atlas of the Western Canada Sedimentary Basin, G. D. Mossop and I. Shetsen (comp.) Calgary, Canadian Society of Petroleum Geologists and Alberta Research Council, 431-438.

*Peirce, J. W., Charters, R. A., and Goussev, S. A., in press, Response to comments by R. Pawlowski on the article by Peirce et al., 1998, Intra-sedimentary magnetization of the Hines Creek Fault (N. Alberta) by vertical fluid flow and exotic geochemistry: The Leading Edge, **17**, 89-92.*

*Peirce, J. W., Goussev, S. A., Charters, R. A., Abercrombie, H. J., and De Paoli, G.R., 1998, Intra-sedimentary magnetization of the Hines Creek Fault (N. Alberta) by vertical fluid flow and exotic geochemistry: The Leading Edge, **17**, 89-92.*

*Reid, A. B., Allsop, J. M., Granser, H., Millett, A. J., and Somerton, I. W., 1990, Magnetic interpretation in three dimensions using Euler deconvolution: Geophysics, **55**, 80-91.*

Ross, G. M., Broome, J., Miles, W., 1994, Potential fields and basement structure - Western Canada Sedimentary Basin, in Geological Atlas of the Western Canada Sedimentary Basin, G. D. Mossop and I. Shetsen (comp.), Calgary, Canadian Society of Petroleum Geologists and Alberta Research Council, 41-47.

*Thompson, D. T., 1982, EULDPH - a new technique for making computer assisted depth estimates from magnetic data: Geophysics, **47**, 31-37.*

*Werner, S., 1953, Interpretation of magnetic anomalies as sheet-like bodies: Sver. Geol. Undersok, ser. C. C. Arsbok **43**, N:06.*

Wright, G. N., McMechan, M. E., and Potter, D. E. G., 1994, Structure and architecture of the Western Canada Sedimentary Basin: in *Geological Atlas of the Western Canada Sedimentary Basin, G. D. Mossop and I. Shetsen (comp.), Calgary, Canadian Society of Petroleum Geologists and Alberta Research Council, 25-40.*

---

[1]Bemex Consulting International, 5288 Cordova Bay Road, Victoria, B.C. V8Y 2L4, Canada

[2]Birch Mountain Resources Limited, Suite 3100, 205-5th Avenue SW, Calgary, Alberta T2P 2V7, Canada

[3]GEDCO, Suite 1200, 815-8th Avenue SW, Calgary, Alberta T2P 3P2, Canada